Fluid Model of Explosive Coalescence

T. Tajima*, J. I. Sakai**

Abstract

Magnetohydrodynamic simulation of the explosive coalescence of magnetic islands is carried out. This result is in agreement with the electromagnetic particle simulation. A theoretical model to describe this process observed in our computer simulations is presented. The theory describes the magnetic collapse and is based on a self-similar solution to the two-fluid plasma equations, as the simulation exhibits temporal self-similarity. The master equation for the scale factor takes a from of the orbital equation in a Sagdeev potential.

I. Introduction and MHD Simulation

In the preceding companion paper[1] on the simulation study of coalescence of magnetic islands we discovered explosive coalescence. In the present paper we further study its magnetohydrodynamic evolution by simulation and analyze the physical processes based on the plasma two-fluid model. The coalescence instability[2] itself is an ideal magnetohydrodynamic (MHD) instability in the linear stage[3]. In nonlinear stages, however, it involves reconnection of field lines and thus non-ideal (or resistive) MHD processes. The reconnection is driven by the ideal MHD instability external to the point of reconnection. In Refs. 4 and 5 the nonlinear process of driven reconnection was analyzed that generalizes the Sweet-Parker process of reconnection. The MHD simulation model we use is the MHD particle code[6] with $2\frac{1}{2}$ dimensions. The configuration of the plasma and magnetic fields is that of Ref.7 based on the initial conditions of Fadeev et al.'s equilibrium[8]. The MHD particle code is robust in applications to problems even with strong turbulence, flows, convections, and density depression. This is helpful because the problem involves fast (explosive) reconnection, strong density depression and compression, and strong flows. The magnetic induction equation is advanced by the Lax-Wendroff method[4]. The plasma is originally uniform in density and temperature contained by metallic (conducting) walls at y $= 0$ and L_y. Here typical parameters are: $L_x/\Delta = 128$ and $L_y/\Delta = 64$, the number of fluid particles 32768, the "poloidal" magnetic fields B_x at $y = 0$ and L_y are such that the ("poloidal") Alfvén velocity $v_{Ap} = 3.5c_s$, the adiabatic constant $\gamma = 2$, and the size of particles $a = 1.0\Delta$, where c_s is the sound speed and Δ is the unit grid length. The current localization parameter ε_c is varied from the value $\varepsilon_c = 0.3$ to 0.85 where ε_c appears in the equilibrium

*Institute for Fusion Studies, University of Texas, Austin, Texas 78712, U.S.A.
**Department of Applied Mathematics and Physics, Toyama University, Toyama, 930 Japan

current profile as $J_z = B_{ox}k(1-\varepsilon_c^2)(\cosh ky + \varepsilon_c \cos kx)^{-2}$. The Alfvén transit times across the y-direction and the x-direction are $\tau_{Ay} = 18.3\Delta/c_s$ and $\tau_{Ax} = 36.5\Delta/c_s$, respectively. The typical magnetic Revnolds number is $R_m \cong 10^4$ with $\eta = 0.036\Delta c_s$. As is well known, the ideal MHD dynamics does not contain any characteristic length, except for the system's overall length; in the present case it is either L_y or the island width. For example, the collisionless skin depth c/ω_{pe} and the Debve length vanish. Therefore, in contrast with the kinetic model discussed in Ref. 1, the spatial scales are not compressed. Similarly the relevant time scales are the Alfvén time and the much larger resistive time. On the other hand, the MHD model largely lacks the kinetic effects such as the Landau and cyclotron dampings, particle acceleration, finite Larmor radius effects, etc. Thus the study the MHD model is complementary to that by the particle simulation model.

Figure 1 shows the kinetic energy and the reconnected flux upon coalescence as a function of time for the case with $\varepsilon_c = 0.85$. A theoretical curve $(t_0 - t)^{-4/3}$ is superimposed on the simulation result. During the rapid increase of reconnected flux ($t \cong 50 - 90\Delta c_s^{-1}$) the simulation result matches reasonably with the theoretical curve. Beyond $t = 90\Delta c_s^{-1}$ the increase begins to be mitigated due to a saturation effect (the flux depletion). In contrast Figs.5-8 in Ref.7 displayed the case with $\varepsilon_c = 0.7$.

The reconnected flux ψ increased rapidly with $\Delta\psi \infty t^m$ ($m \sim 1.9$). It was, however, less rapid than the case with $\varepsilon_c = 0.85$. The released energy was also less in the present case. In Ref.7 the case with $\varepsilon_c = 0.3$ was also treated, where $\Delta\psi \infty t^m$ with $m = 1$. Thus, it is clear that as ε_c increases, the process of reconnection becomes faster, changing from the Sweet-Parker rate $(\varepsilon_c = 0.3)^3$ to the faster rate $(\varepsilon_c = 0.7)^{4.7}$ to the explosive rate $(\varepsilon_c = 0.85)$. It is to be noted that pulsations are seen that are superimposed on the overall growth of the reconnected flux in Fig.1 as well as in Fig.5 and 7 of Ref.7. The pulsations in Fig.1 are more irregular than the ones in Fig.5 and 7 in Ref.7. The period of these pulsations is of the order of the poloidal Alfvén transit time in the x-direction.

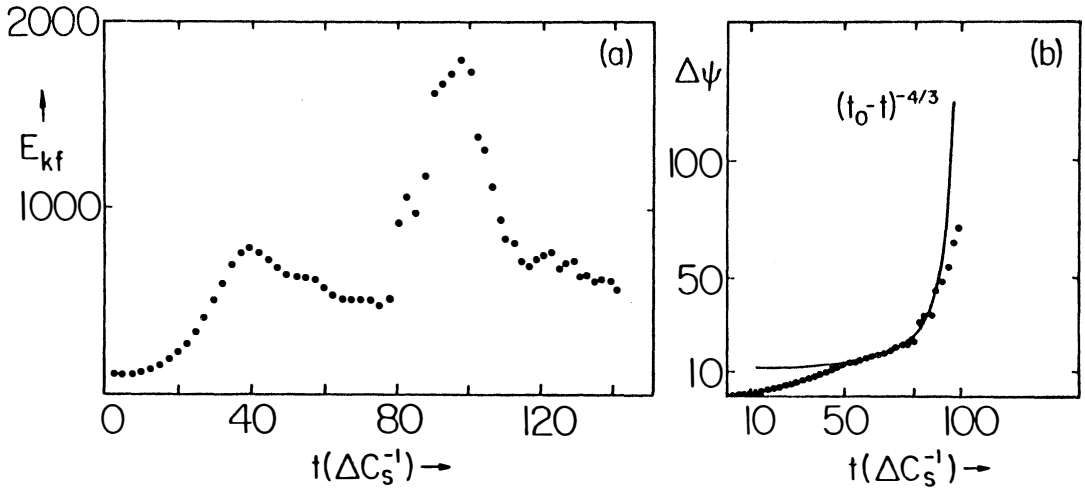

1. Temporal profiles of the fluid energy (a) and the reconnected flux (b) for $\varepsilon_c = 0.85$ obtained from the MHD particle simulation. A solid line in (b) is a theoretical curve.

The structure and its evolution of the plasma and magnetic fields during the coalescence are now examined. The case of $\epsilon_c = 0.7$ is shown in Figs.2 and 3, while that of $\epsilon_c = 0.85$ in Fig.4. Compared are two time stages: Fig.2 just about at the beginning of rapid coalescence and Fig.3 during the continued rapid coalescence. The sequence of coalescence proceeds as follows. The early slight displacement toward each island is shown in Fig.2(a) at $t = 20\Delta/c_s$. When the two islands come in full contact, the magnetic field lines exhibit a pattern similar to that shown in Fig.1(b) of Ref.7. At this moment $(t = 40)$, the plasma density at the x-point becomes high (about twice as the original value) as shown in Fig.2(c) at the same time the current (J_z) is strongly induced at the x-point as seen in Fig.2(b). The plasma flow is shown in Fig.2(d), exhibiting inflows along the x-direction and strong jet outflows aiong the y-direction making an overall pattern of vortices. The plasma flow in the z-direction is shown in Fig.2(e): As the x-y flows are set up by the coalescence, the z-direction flow is induced because of the toroidal field. The development so far is qualitatively similar to the case of $\epsilon_c = 0.3$ (except that the islands squeeze the plasma in between a little more and the sheet structure is thinner here).

However, later (at $t = 75$) there appear some deviations from the $\epsilon_c = 0.3$ case. Figure 3 shows the snapshot of the flux, current, density, flow in the x-y-plane, and the flow in the z-direction at $t = 75\Delta/c_s$. Note that an x-point-like feature appears at $x = 64\Delta$, $y = 32\Delta$ as well as a marked and rapid density variation in the plasma sheet [see Figs.3(a) and (c)]: The flow has a very large value near the x-point and inner vortex structure[Fig.3(d)]. Note also that this

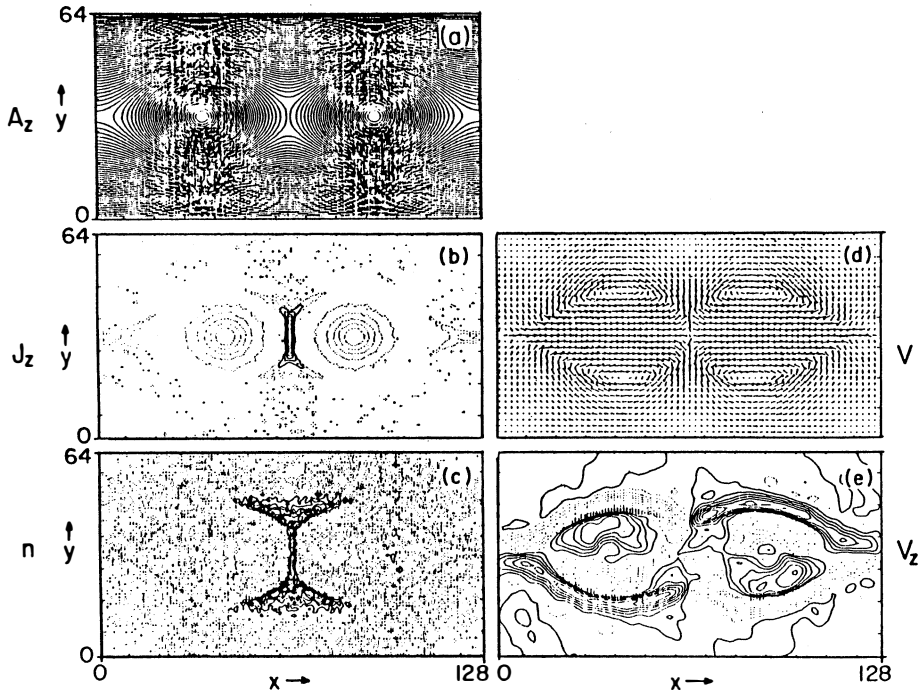

2. Spatial structure of plasma and fields "before" coalescence with $\epsilon_c = 0.7$.(a) magnetic field lines at $t = 20\Delta c_s^{-1}$. (b) Toroidal current density J_z contours. (c) Plasma density. (d) Plasma flow velocity. (e) Plasma z-direction flow velocity contours. (b)-(e) at $t = 40\Delta c_s^{-1}$: Solid lines correspond to above-average contours and dotted once to below-average.

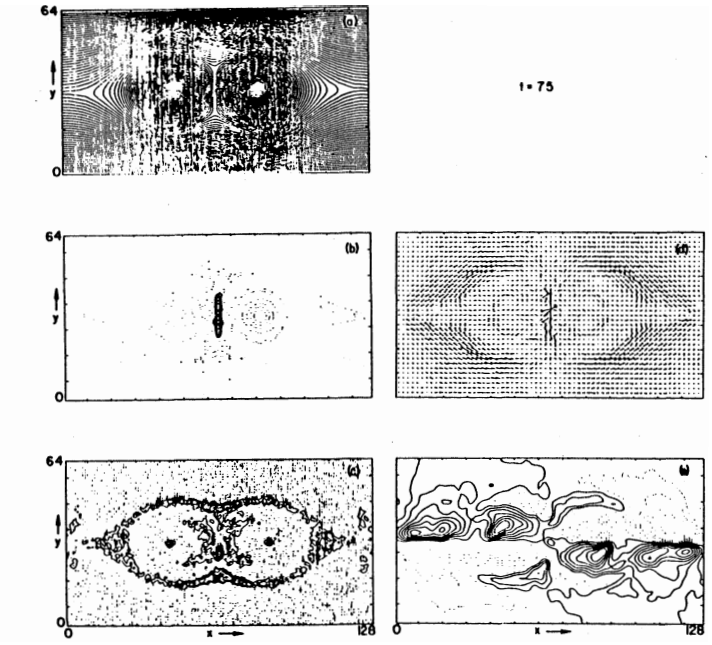

3. Spatial structure of plasma and fields "during" coalescence with $\varepsilon_c = 0.7$. (a)-(f) as indicated for Fig.2.(a)-(e) at $t = 75\Delta c_s^{-1}$.

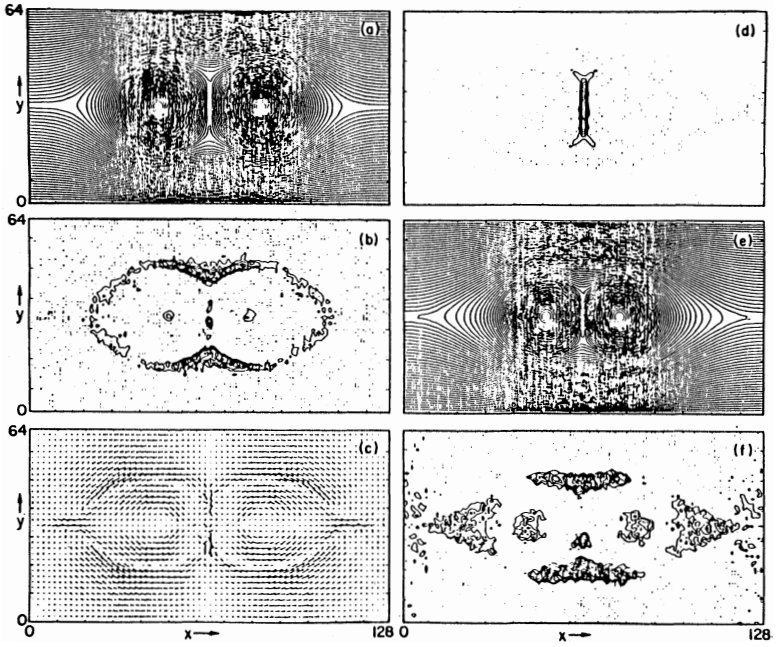

4. Spatial structure of plasma and fields "before" and "during" coalescence with $\varepsilon_c = 0.85$. (a) Magnetic field lines. (b) Plasma density contours. (c) Plasma flow velocities. (d) Current density (J_z) contours. (a)-(d) at $t = 50\Delta c_s^{-1}$. (e) Magnetic field lines. (f) Plasma density contours. (e) and (f) at $t = 87.5\Delta c_s^{-1}$.

($t = 75$) is the period during which the continuous rapid coalescence goes on. These features were not observed in the case $\varepsilon_c = 0.3$ (see Fig.1, Ref.7), in which the reconnected flux increased linearly in time and in proportion with the square root of the resistivity η ($\Delta\psi \propto \eta^{1/2} t$) and in which the reconnection angle stayed very narrow.

These signatures are consistent with our hypothesis(a) that the reconnection takes place by the mechanism of Sweet and Parker for coalescence with $\varepsilon_c = 0.3$. The signatures found in Fig.3, on the other hand, imply that the reconnection process is not that of Sweet and Parker. It shows instead that(i) the reconnection angle at the x-point has enlarged [Fig.3(a)]; (ii) a high density spot near the x-point is formed [Fig.3(c)]; (iii) the reconnected flux increases faster than the Sweet-Parker process ($\Delta\psi \propto t^m$ with $m \sim 2$). These are consistent with our futher hypothesis (b) that the reconnection is through the process of Brunel, Tajima and Dawson[4] for coalescence with $\varepsilon_c = 0.7$. ($t = 160$), the system approaches saturation when most of the flux available has reconnected. The flow is randomized.

Figure 4 presents the pattern of the plasma and fields of the case $\varepsilon_c = 0.85$, where we see faster and explosive reconnection corresponding to Fig.1. We are advancing our third hypothesis(c) that the coalescence with $\varepsilon_c = 0.85$ is explosive. See Table I. In frames of Figs.4(a)-(d) ($t = 50$) one sees the coalescence behavior before it becomes explosive. Although, in Figs.4(a) and (b), in particular, one can detect some deviation from the Sweet-parker type for $\varepsilon_c = 0.3$, it is qualitatively similar to the $\varepsilon_c = 0.3$ case and the $\varepsilon_c = 0.7$ case at this stage. In Figs.4(e) and (f) ($t = 75$), we now see significant devitions in pattern from the cases with less ε_c. A much wider reconnection angle than the previous ones is observed in Fig.4(e). From these observations it can be argued that the widening of the reconnection angle has to be accompanied by fast or explosive coalescence. This is in agreement with the suggestion made in Ref.4.

Ⅱ. Theoretical Model

Geometry of magnetic fields here is exemplified by Fig.3(a). We are primarily concerned with the plasma sheet region (in the neighborhood of $x = 64\Delta$ and $y \sim 20\Delta - 42\Delta$). In the vicinity of the sheet region the physics is nearly one-dimensional, that is, the variation of quantities in the y-direction is much less than that in the x-direction. We further generalize the discussion of Ref.4 in the following. The main generalization in the present theory beyond Ref.4 is the replacement of the pressure equilibrium by the dynamical equation of motion. We assume that $\partial/\partial x \gg \partial/\partial y, \partial/\partial z$, in which x is the direction of coalescence, while y is the direction of "poloidal" magnetic field line and z is the direction of plasma current.We treat the external plasma dynamics of the explosive stage as a one-dimensional problem. Toward the end of this section we comment on two-dimensional effects, however.

We start from the two-fluid model equations of plasma and the Maxwell equations, neglecting the displacement current. We assume the adiabatic law of states for both electrons and ions. The basic equations read as follows:

$$\frac{\partial n_j}{\partial t} + \nabla \cdot (n_j \boldsymbol{v}_j) = 0 \qquad (1)$$

$$m_j n_j \frac{d\boldsymbol{v}_j}{dt} = n_j e_j \left(\boldsymbol{E} + \frac{\boldsymbol{v}_j}{c} \times \boldsymbol{B} \right) - \nabla p_j, \tag{2}$$

$$\nabla \times \boldsymbol{B} = \frac{4\pi}{c} \sum_j n_j e_j \boldsymbol{v}_j, \tag{3}$$

$$\nabla \times \boldsymbol{E} = 4\pi \sum_j n_j e_j, \tag{4}$$

$$\nabla \times \boldsymbol{E} = -\frac{1}{c} \frac{\partial \boldsymbol{B}}{\partial t} \tag{5}$$

$$\frac{\partial p_j}{\partial t} + \boldsymbol{v}_j \cdot \nabla p_j + \gamma p_j div\ \boldsymbol{v}_j = 0, \tag{6}$$

where j denotes the species of particles and γ is the ratio of heat capacity which is related to the degree of the system f as $\gamma = 1 + 2f$. The appropriate choice of γ in Eq. (6) depends on individual cases and models we use.[1] For example, the explosive process observed in the kinetic simulation showed a strong one dimensional (one directional) acceleration, which gives rise to one degree of motion $f = 1$ and thus to $\gamma = 3$. On the other hand, in the MHD simulation, the adiabatic constant γ for electrons was fixed to be 2.

During explosive coalescence, there is no specific scale length. The scale length characterizing the current sheet varies continuously in time without deformation of global structure of current sheet. If one looks at the evolution of the system locally in time, the system undergoes the rapid field and temperature rise, compression of plasma, change of the reconnection angle etc. in a certain specific fashion which was detailed in the preceding paper.[1] If one looks at the same system locally in time a little later, the system undergoes these changes with different magnitudes, but still in the same specific fashion. That is, the relations that govern the explosive coalescence themselves are invariant under the change of time scale. This was the manifestation of the presence of self-similarity in the system during explosive coalescence. Such a physical situation may best be described by self-similar solutions in which scale factors vary continuously.

We introduce scale factors $\mathrm{a}(t)$ and $\mathrm{b}(t)$ as follows,

$$v_{ex} = \frac{\dot{a}}{\mathrm{a}} x, \tag{7}$$

$$v_{ix} = \frac{\dot{b}}{b} x, \tag{8}$$

where a dot represents the time derivative. An ansatz is imposed here that the velocities are linear in x. The linear dependence on x of the velocities implies that particles flow in the opposite direction around the center of current sheet, $x = 0$. The scale factors a and b will be determined from the above basic equations. From the continuity equations of electrons and ions, Eq. (2), we obtain

$$n_e = n_0/a, \tag{9}$$

$$n_i = n_0/b, \tag{10}$$

where n_0 is a constant. Equations (9) and (10) show that the densities of ions and electrons are

nearly homogeneous in space and vary only in time during coalescence. The self-similar solutions obtained here are local solutions in space whose properties are dominated by the physical process near the current sheet. We therefore neglect the higher terms in space proportional to x^3 and higher hereafter. The current J_z in the sheet is nearly constant. This means that as n is nearly constant, v_z is also approximately constant in space. Neglecting the term with x^3 in Eq. (3), we obtain

$$\frac{B_0(t)}{\lambda} = \frac{4\pi e n_0}{c}\left(\frac{v_{iz}^{(0)}}{b} - \frac{v_{ez}^{(0)}}{a}\right), \tag{11}$$

where we assumed the magnetic-field B_y varies as $B_y = B_0(t)\frac{x}{\lambda}$, where λ is the magnetic field scale length. This ansatz is consistent with the assumption that the sheet current is (nearly) constant in space.

From the y-component of Eq.(5) and the z-component of equation of motion for electrons Eq. (2) we obtain

$$\dot{B}_0 = 2c\frac{E_{z1}}{\lambda}, \tag{12}$$

$$E_{z1}\frac{x^2}{\lambda^2} + \frac{\dot{a}}{a}\cdot\frac{B_0(t)}{\lambda c}x^2 = 0, \tag{13}$$

$$\frac{\partial v_{ez}^{(0)}}{\partial t} = -\frac{e}{m_e}E_{z0}, \tag{14}$$

where

$$E_z = E_{z0}(t) + E_{zl}(t)\frac{x^2}{\lambda^2} \tag{15}$$

Equations (12) and (13) yield

$$B_0(t) = \frac{B_{00}}{a^2}, \tag{16}$$

Assuming that the electrostatic field E_x varies like $E_x = E_0(t)\,x/\lambda$, we obtain from Poisson's equation (4)

$$E_0 = 4\pi e n_0 \lambda\left(\frac{1}{b} - \frac{1}{a}\right), \tag{17}$$

Furthermore, the equations of state for electrons and ions give rise to

$$P_e = \frac{P_{0e}}{a^\gamma} - \frac{P_{0e}}{2a^{\gamma+2}}\cdot\frac{x^2}{\lambda^2}, \tag{18}$$

$$P_i = \frac{P_{0e}}{b^\gamma} - \frac{P_{0e}}{2b^{\gamma+2}}\cdot\frac{x^2}{\lambda^2}, \tag{19}$$

We now go back to the x-component of equations of motion for electrons and ions in order to obtain the basic equations for $a(t)$ and $b(t)$. If we neglect the small terms of the order of the mass ratio m_e/m_i, we obtain

$$\ddot{a} = -\omega_{pe}^2\left(\frac{a}{b} - 1\right) - \frac{B_{00}^2}{4\pi m_e n_0 \lambda^2 a^2} + \frac{P_{0e}}{m_e n_e \lambda^2 a^\gamma}, \tag{20}$$

$$\ddot{b} = \omega_{pi}^2\left(1 - \frac{a}{b}\right) + \frac{P_{0i}}{m_i n_0 \lambda^2 b^\gamma}, \tag{21}$$

Furthermore, assuming that the plasma is quasi-neutral $n_i = n_e$, i.e.,$a = b$, by adding Eqs.(20) and (21)

$$\ddot{a} = -\frac{v_A^2}{\lambda^2 a^2} + \frac{c_S^2}{\lambda^2 a^\gamma}, \tag{22}$$

where v_A and c_s are the Alfvén and sound velocities. In Eq.(22) the first term of the RHS corresponds to the $J \times B$ term. This is the term that drives magnetic compression (pollapse). The second term corresponds to the pressure gradient term. This term may eventually be able to balance the magnetic collapse when $\gamma = 3$.

Once the behavior of the scale factor $a(t)$ is determined from the above equations, we obtain various kinds of physical quantities as follows, in the quasi-neutral plasmas, and neglecting the mass ratio $\left(\frac{m_e}{m_i} \to 0\right)$,

$$B_y = \frac{B_{00}}{a^2} \cdot \frac{x}{\lambda} \tag{23}$$

$$E_x = \left(-\frac{m_i v_A^2}{e\lambda a^3} + \frac{P_{0e}}{e\lambda a^4 n_0}\right)\frac{x}{\lambda} \tag{24}$$

$$E_z = \frac{B_{00}\dot{a}x^2}{ca^3\lambda} - \frac{B_{00}m_e c\dot{a}}{4\pi n_0 e^2 \lambda a^2} \tag{25}$$

$$v_{ez} = -\frac{cB_{00}}{4\pi n_0 e^2 \lambda a^2} \tag{26}$$

$$v_{ix} = v_{ex} = \frac{\dot{a}}{a}x \tag{27}$$

$$n_i = n_e = \frac{n_0}{a} \tag{28}$$

where the electrostatic field E_x in the quasi-neutral plasmas is determined from the equation of motions for ions, not from Poisson's equations. From Eqs.(23) and (24) we find a result that in the explosive phase $(a \to 0)$ the electrostatic field $[E_x \propto (a^{-3} + a^{-4})]$ grows more rapidly than the magnetic field $(B_y \propto a^{-2})$ does.

Now we investigate the global time behavior of coalescence by making use of the first integral of Eq.(22). Equation(22) is rewritten as

$$\ddot{a} = -\frac{\partial V(a)}{\partial a}, \tag{29}$$

where $V(a)$ is the effective (Sagdeev) potential. The schematic graph of the effective potential is drawn in Fig.5(a). The value a which satisfes $V(a_1) = 0$ is given by $a_1 = \frac{1}{2}\beta$, with $\beta \equiv c_s^2/v_A^2$. The minimun of the potential, $V_{\min}$, $V_{\min} = \frac{-v_A^4}{2\lambda^2 c_s^2}$, at $a = 2a_1 = \beta$. For low β the driving force $J \times B$ is dominant compared with the pressure term. The first integral of Eq.(29) is given by

$$\dot{a}^2 = \frac{2v_A^2}{\lambda^2 a} - \frac{c_s^2}{\lambda^2 a^2} + \varepsilon, \tag{30}$$

where $\varepsilon/2$ is the initial (Sagdeev) "energy." As seen from Fig.5(a), the explosive magnetic compressin corresponds that the scale factor $a(t)$ rapidly changes in time by orders of magnitude and nearly vanishes. Such an explosive collapse can be realized (i) when the β is small; (ii) when the intial total energy $\varepsilon/2$ is nearly zero.

Let us examine the time history of yarious physical quantittes based on the qualitative time behavior of $a(t)$ derivable from the effective potential $V(a)$. The magnetic field energy is prop-

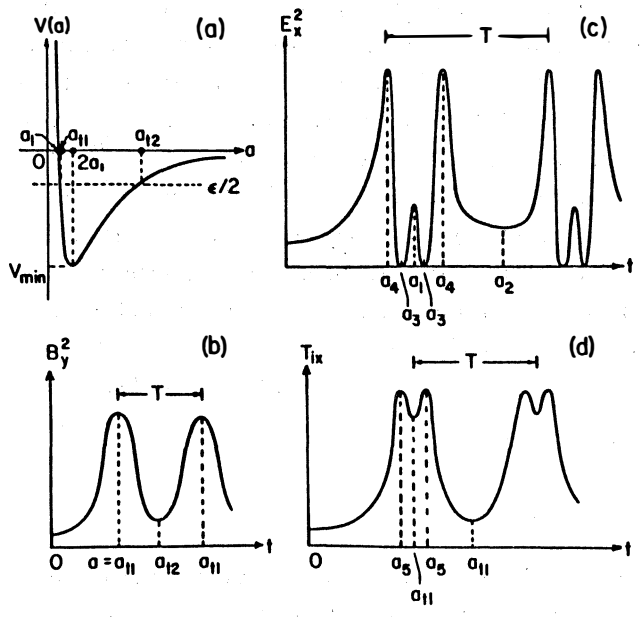

5. Behavior of explosive coalescence. (a) The Sagdeev potential for the scale factor a. (b) The temporal profile of the magnetic energy. (c) That of the electrostatic field energy. (d) That of the ion temperature in the x-direction.

ortional to B_y^2, which is given by $B_y^2 = \frac{B_{00}^2}{a^4}\left(\frac{x}{\lambda}\right)^2$. If the scale factor a becomes smaller, B_y^2 must increase. The maximum is given by $\frac{\partial B_y^2}{\partial t} = 0$, which yields $\dot{a} = 0$ at $a = a_{t1}$. After the maximum, B_y^2 decreases again and reaches minimum at $a = a_{t2}$. The oscillatory behavior of the magnetic field energy is schematically drawn in Fig.5(b).

The electrostatic field E_x is given by Eq.(24). The time history of the electrostatic field energy, which is propositional to E_x^2, is analyzed by investigating $\frac{\partial E_x^2}{\partial t} = 0$. This condition is equivalent

$$\epsilon_0 = 0, \qquad \text{or} \qquad \frac{\partial \epsilon_0}{\partial t} = 0 \tag{31}$$

where $\epsilon_0(t) = -\frac{m_i v_A^2}{e\lambda a^3} + \frac{P_{0e}}{e\lambda n_0 a^4}$. The first condition $\epsilon_0 = 0$ occurs at $a = a_3 \simeq \beta$. The second condition $\partial\epsilon_0/\partial t$ gives two conditions: (i) $\dot{a} = 0$, $a = a_{t1}$, a_{t2} or (ii) $a = a_4 = 4\beta/3$.

The above considerations give us the schematic time history of the electrostatic field energy E_x^2 as drawn in Fig.5(c). Figure5(c) indicates a triple-peak structure in the electrostatic field energy. When the plasma β is small, a^3 and a_{t1} are close. In this case, the triple-peak structure in the electrostatic field energy world become double-peak structure.The maximum value of the electrostatic field, $E_{\max}$, achieved at $a = a_4$ is given by

$$E_{\max} = \frac{1}{4}\left(\frac{3}{4}\right)^3 \frac{m_i v_A^8 x}{e\lambda c_s^6 \lambda}. \tag{32}$$

The induced electric field E_z is given by Eq.(25), which shows that E_z becomes zero, when $\dot{a} = 0$. E_z changes its sign around $\dot{a} = 0$ because $\dot{a} = 0$ is the point where the magnetic field achieves maximum or minimum.

Next, the time behavior of ion temperature T_{ix} is examined. In the early stage of coalescence, the plasma should be adiabatically compressed. However, as the magnetic field energy increases near the peak and approaches the peak, the ion flow energy becomes dominant over the thermal energy. From the consideration that ${v_x}^2$ gives maximum or minimum, namely $\frac{\partial {v_x}^2}{\partial t} = 0$, we find two conditions for the extrema; (i) $v_x = 0$, which gives $\dot{a}$, (ii) $\frac{\partial v_x}{\partial t} = 0$, which gives $a\ddot{a} = \dot{a}^2$. When the explosive coalescence takes place ($\epsilon = 0$), this leads to the condition $a = a_5 \simeq 2\beta/3$. After $a = a_5$, the kinetic energy must decrease, which means that the plasma is in the state of colliding phase. The above considerations give us the schematic time history of the ion temperature, which is shown in Fig.5(d). Figure5(d) shows a doublepeak structure in the ion temperature. The temperature T is given by $T = P/n$, while the dominant term in pressure changes in time as $P \sim a^{-5}$ when $\gamma = 3$, $P \sim a^{-4}$ when $\gamma = 2$, while $n \sim a^{-1}$. Therefore we find

$$T = \frac{P}{n} \simeq \frac{1}{a^4} (\gamma = 3), \tag{33}$$

$$\simeq \frac{1}{a^3} (\gamma = 2).$$

We investigate in more detail the explosive phase of the coalescence in a case where we can neglect the effect of plasma pressure: it only acts as a saturation mechanism. The solution of Eq.(22) with ${c_s}^2 = 0$, small ϵ and $\gamma = 3$ is given by

$$a(t) \cong \left(\frac{9}{2}\right)^{1/2} \left(\frac{v_A}{\lambda}\right)^{2/3} (t_0 - t)^{2/3} + 0(\epsilon) \tag{34}$$

where we neglect the order of ϵ and t_0 is the explosion time. Once the solution $a(t)$ is given by Eq.(34), we can find the various physical quantities as follows, which is valid in the explosive phase of the coalescence;

$$v_x = v_{ix} = v_{ex} = -\frac{2}{3} \cdot \frac{x}{(t_0 - t)}, \tag{35}$$

$$n = n_i = n_e = \left(\frac{2}{9}\right)^{1/3} \frac{\lambda^{2/3} n_0}{{v_A}^{2/3} (t_0 - t)^{2/3}}, \tag{36}$$

$$E_x = -\frac{2}{9} \cdot \frac{m_i}{e} \cdot \frac{x}{(t_0 - t)^2}, \tag{37}$$

$$B_y = \left(\frac{2}{9}\right)^{2/3} \frac{B_{00} \lambda^{1/3} x}{{v_A}^{4/3} (t_0 - t)^{4/3}}, \tag{38}$$

$$E_z = \frac{2}{3} \left(\frac{2}{9}\right)^{2/3} \frac{B_{00} \lambda^{1/3} x^2}{{v_A}^{4/3} c (t_0 - t)^{7/3}} + \frac{2}{3} \left(\frac{2}{9}\right)^{1/3} \frac{B_{00} c}{{\omega_{pe}}^2 \lambda^{1/3} {v_A}^{2/3} (t_0 - t)^{5/3}}. \tag{39}$$

Let us compare the theoretical results obtained here with the computer simulatton results. The global structure of the magnetic field energy, electrostatic field energy, and ion temperature in the x-direction observed in the simulation is well explained by the theoretical model obtained here. Especially, the double-peak structure in the ion temperature and the triple-peak structure in the electrostatic field energy are also observed in the simulation (see Figs.2 and 3 in the preceding paper)[1]. Table I of Ref.1 summarized the results of comparison of the explosion indices between the theory and the collisionless simulation.

Table 1 Coalescence and Current Peakedness (ε_c)

ε_c	0	0.3	0.7	0.85
Process	Sheet pinch tearing instability	Slow Coalescence Sweet-Parker process	Fast Coalescence	Explosive Coalescence
Reconnecting. flux $\Delta\psi$	$e^{\gamma_L t}$ $\gamma_L \propto \eta^{3/5}$	$\eta^{1/2}t$	$\eta^{1/2}t^m$ (m $\geq$ 1)	$\eta^0/(t_0-t)^{4/3}$

In Table I of Ref.1 we showed the index m of explosiveness [tte exponent to the time $(t_0-t)^{-m}$], in good agreement between simulation and theory in the electrostatic energy. The electrostatic field energy, magnetic field energy, and ion temperature are well explained by the one-dimensional model of the explosive collapse.

Comments are made on two-dimensional effects. We introduce four scale factors $a(t)$, $b(t)$, $c_1(t)$ and $d(t)$ as follows

$$v_{ix} = \frac{\dot{a}}{a}x,$$

$$v_{iy} = \frac{\dot{b}}{b}y,$$

$$v_{ex} = \frac{\dot{c}_1}{c_1}x,$$

$$v_{ey} = \frac{\dot{d}}{d}y. \tag{40}$$

From the equations of motion for electrons and ions we finally obtain for a, b, c_1, and d

$$\ddot{a} = \omega_{pi}^2 \left(\frac{\lambda_2}{\lambda_1+\lambda_2}\right)\left(\frac{1}{b}-\frac{a}{c_1 d}\right) \tag{41}$$

$$\ddot{b} = \omega_{pi}^2 \left(\frac{\lambda_1}{\lambda_1+\lambda_2}\right)\left(\frac{1}{a}-\frac{b}{c_1 d}\right) \tag{42}$$

$$\ddot{c}_1 = -\omega_{pe}^2 \left(\frac{\lambda_2}{\lambda_1+\lambda_2}\right)\left(\frac{c_1}{ab}-\frac{1}{d}\right) - \frac{v_{Ae}^2}{\lambda^2}\left(\frac{d}{c_1^2}-\frac{1}{d}\right) \tag{43}$$

$$\ddot{d} = -\omega_{pe}^2 \left(\frac{\lambda_1}{\lambda_1+\lambda_2}\right)\left(\frac{d}{ab}-\frac{1}{c_1}\right) + \frac{v_{Ae}^2}{\lambda^2}\left(\frac{1}{c_1}-\frac{c_1}{d_2}\right). \tag{44}$$

The quasi-neutrality $(n_i = n_e)$ imposes that "Wronskian" being zero, $ab = c_1 d$. These equations were first derived by Imshenik and Syrovatskii.[9] In the limit of $t \to t_0$ we have approximately

$$c_1 \simeq (t_0-t)^{2/3} \quad \text{and} \quad d \approx \text{constant}. \tag{45}$$

This reduces to the one-dimensional results discussed in the above.

Roseneau also obtained a self-similar two-dimensional solution.[10] Recently we have come to learn that Kadonaga and Tomimatsu[11] obtained solutions similar to Eqs.(35)-(39).

We would like to thank Drs.F.Brunel, A.Bhattacharjee, and A.G.Litvak for their helpful discussions on the manuscript. This work is supported by the U.S.Department of Energy and the National Science Foundation.

References

1. T. Tajima and J.I. Sakai, accompanying paper.
2. J.M. Finn and P.K. Kaw, Phys. Fluids **20**, 72 (1977).
3. P.L. Pritchett and C.C. Wu, Phys. Fluids **22**, 2140 (1979).
4. F. Brunel, T. Tajima, and J.M. Dawson, Phys. Rev. Lett. **49**, 323 (1982).
5. S.I. Sylovatskii, Sov. Phys. JETP **33**, 933 (1971) [Zh. Eksp. Teor. Fiz. **60**, 1727 (1971)].
6. J.N. Leboeuf, T. Tajima, and J.M. Dawsbon, J. Comp. Phys. **31**, 379 (1979).
7. A. Bhattacharjee, F. Brunel, and T. Tajima, Phys. Fluids **26**, 3332 (1983).
8. V.M. Fadeev, I.F. Kvartsvkawa, and N.N. Komarov, Nucl. Fusion **5**, 202 (1965).
9. V.S. Imshenik and S.I. Syrovatskii, Sov. Phys. JETP **25**, 656 (1967) [Zh. Ek. Teor. Fiz. **52**, 990 (1967)].
10. P. Roseneau, Phys. Fluids **22**, 848 (1979).
11. Kadonaga and Tomimatsu, Prog.Theor. Phys. **63**, 1202 (1980).

(Received October, 31 1988)